Articles
doi.org/10.1002/batt.202000027

Chemistry Europe
European Chemical Societies Publishing

Amine- and Amide-Functionalized Mesoporous Carbons: A Strategy for Improving Sulfur/Host Interactions in Li–S Batteries

Samuel J. Fretz[+],[a] Marco Agostini[+],*[b] Piotr Jankowski,[b, c] Patrik Johansson,[b] Aleksandar Matic,[b] and Anders E. C. Palmqvist*[a]

Lithium–sulfur (Li–S) batteries are of great interest due to their potentially high energy density, but the low electronic conductivity of both the sulfur (S_8) cathode active material and the final discharge product lithium sulfide (Li_2S) require the use of a conductive host. Usually made of relatively hydrophobic carbon, such hosts are typically ill-suited to retain polar discharge products such as the intermediate lithium polysulfides (LiPs) and the final Li_2S. Herein, we propose a route to increase the sulfur utilization by functionalizing the surface of ordered mesoporous carbon CMK3 with polar groups. These derivatized CMK3 materials are made using a simple two-step procedure of bromomethylation and subsequent nucleophilic substitution with amine or amide nucleophiles. We demonstrate that, compared to the unfunctionalized control, these modified CMK3 surfaces have considerably larger binding energies with LiPs and Li_2S, which are proposed to aid the electrochemical conversion between S_8 and Li_2S by keeping the LiPs species in close proximity to the carbon surface during Li–S battery cycling. As a result, the functionalized cathodes exhibit significantly improved specific capacities relative to their unmodified precursor.

1. Introduction

New electrochemical energy storage systems are needed urgently to satisfy the growing demand of portable electronics market.[1–4] While lithium–sulfur (Li–S) batteries are considered one of the most attractive candidates among next generation battery concepts, owing to their potentially high energy density, low raw materials cost, and low toxicity,[5,6] their practical application has been limited so far by several issues related to the electric conductivity and solubility of sulfur, the active material of the Li–S battery cathode, and its discharge products.[7] Elemental sulfur (S_8) and its discharge products, lithium disulfide (Li_2S_2) and lithium sulfide (Li_2S), are intrinsically insulating and are typically poorly soluble in the battery electrolyte, hence limiting the active material utilization and the electron transport within the cathode.[8–13] In contrast, the partially reduced intermediates, various lithium polysulfides (LiPs, Li_2S_n, $3 \leq n \leq 8$), typically dissolve well in the electrolyte[14] during cell cycling, allowing for more efficient use of the active material, but this also allows the LiPs to diffuse to the surface of the Li metal anode, causing loss of active material and reducing the cycle-life of the battery. To address these problems, the sulfur is usually contained within a porous conductive host, many times carbon, in order to create short-distance conduction paths and limit its diffusion;[6,15,16] while the electrolyte chemistry is tailored with additives[17] and Li–S battery configuration modified using interlayer at the cathode side for mitigating LiPs shuttle effect.[18]

In order to accommodate all the sulfur species effectively, the properties of the carbon host can, in addition, be modified. Its effectiveness as a host depends not only on its porosity and surface area, but also on its surface chemistry and elemental composition.[19] For example, while S_8 is non-polar and can adsorb relatively well on the hydrophobic carbon surface, Li_2S and the intermediate LiPs are strongly polar and therefore adsorb more poorly.[20] The carbon's surface chemistry can be modified *via* a few methods including heteroatom doping, in which nitrogen is the most common dopant.[21–25] Nevertheless, the high temperatures associated with carbon synthesis (typically $> 500\,^{\circ}C$) limit the types of functional groups one can introduce and usually more than one type of functionality is produced (*e.g.* graphitic, pyrrolic, and pyridinic nitrogen). Importantly for LiPs and Li_2S adsorption, there is no guarantee that the nitrogen dopants are present at the carbon surface.

An alternative approach involves the covalent attachment or grafting of small, polar functional groups directly to the carbon surface.[26–29] Such a method is amenable to installing more diverse organic functionality compared to heteroatom doping due to the lower temperatures involved and previous

[a] *Dr. S. J. Fretz,[+] Prof. A. E. C. Palmqvist*
Department of Chemistry and Chemical Engineering
Chalmers University of Technology,
41296 Göteborg, Sweden
E-mail: anders.palmqvist@chalmers.se
[b] *Dr. M. Agostini,[+] Dr. P. Jankowski, Prof. P. Johansson, Prof. A. Matic*
Department of Physics
Chalmers University of Technology,
41296 Göteborg, Sweden
E-mail: agostini@chalmers.se
[c] *Dr. P. Jankowski*
Department of Energy Conversion and Storage
Technical University of Denmark,
2800 Kgs. Lyngby, Denmark
[+] *These authors contributed equally to this work.*

Supporting information for this article is available on the WWW under https://doi.org/10.1002/batt.202000027

work has shown that such modifications impart benefits to the sulfur cathode.[6,11,20] It is postulated that these groups help the relatively hydrophobic carbon host bind to the polar sulfur discharge products (LiPs, Li_2S). Among potential functional groups to graft, carbonyl groups (C=O) have been shown to have the highest binding energies to Li_2S and LiPs.[30] Work from the Cui group has shown that carbon electrodes modified with carbonyl-containing polyamides can render strong interactions between the carbon surface and the polar LiPs, yielding very stable battery cycling.[20] However, the use of a bulky polymer can cause non-uniform functionalization and pore blockage, rendering lower sulfur use. An alternative approach for installing monomeric carbonyl/amide groups on the carbon surface could therefore be advantageous.

The bromomethylation reaction has been reported as the first of a simple two-step carbon functionalization scheme.[31] Compared to other, more common surface modification techniques of carbon materials such as oxidation and diazonium salt coupling, this two-step procedure boasts distinct advantages such as stable surface groups, monolayer coverages, negligible damage to the carbon framework, minimal loss of surface area and porosity, and, importantly, amenability towards a wide range of nucleophiles, allowing diverse functional groups to be installed on the carbon surface.

Herein, we use this two-step scheme to install monomeric amide groups directly onto the mesoporous carbon surface. Subsequently, we investigate, both experimentally and computationally, if amide and amine surface groups improve significantly the retention of the sulfur discharge products to the carbon surface, aiming to enhance capacities and overall cell performance when used as cathodes in Li–S batteries.

2. Results and Discussion

As the substrate for surface groups, we selected ordered mesoporous carbon CMK3 because it has been used extensively as a sulfur host in Li–S batteries.[15,31,32] CMK3 also has a high surface area (830 $m^2 g^{-1}$) and a large pore volume (1 $cm^3 g^{-1}$) due to its mesopores (average diameter at *ca.* 40 Å), allowing for the deposition of a large amount of sulfur. A single 10-g batch of CMK3 was bromomethylated to provide sufficient starting material, denoted Br-CMK3, for all nucleophilic substitution reactions. As a reference to the previous study, 2-g of Br-CMK3 was boiled in neat ethylenediamine (EN) to form a diamine-terminated surface and is denoted EN-CMK3 (Figure 1 and Figure S1).

To synthesize an amide-terminated surface, an amide nucleophile can be formed *in-situ* by addition of strong base at low temperatures (−8 °C) in tetrahydrofuran (THF) solution in the presence of Br-CMK3. The amide nucleophile displaces bromide on Br-CMK3 and forms a covalent bond to the surface. We selected two amide nucleophiles, N,N-dimethylacetamide (DMA) and N,N,N′,N′-tetramethylmalonamide (TMMA), which contain a monoamide and a diamide, respectively. The DMA- and TMMA-substituted samples are referred to as DMA-CMK3 and TMMA-CMK3, respectively (Figure 1). Further details related to these synthetic procedures are reported in the experimental section and Figure S2 and Figure S3.

To assess the success of the nucleophilic substitution reactions, the resulting functionalized carbons were studied through X-ray fluorescence (XRF, Table S1) and elemental analysis (EA, Table S2). The Br-CMK3 starting material shows a bromine loading of 0.65 mmol g^{-1} as determined by XRF, which is reduced to 0.14, 0.20, and 0.27 mmol g^{-1} for EN-, DMA-, and TMMA-CMK3, respectively. Simultaneously, the surface group loadings as determined by nitrogen EA increase to 0.91, 0.74 and 0.37 mmol g^{-1} along the same series and the corresponding yields are 140%, 115%, and 57% (based on initial Br loadings). The yields and residual bromine loadings show that, under the conditions used, EN is the best nucleophile for substituting Br, followed by DMA then TMMA. Thus, as expected, even with higher temperatures and concentrations during the nucleophilic substitution step (see experimental section for details), the bulkier TMMA is an inferior nucleophile relative to DMA. In the case of EN- and DMA-CMK3, the >100%

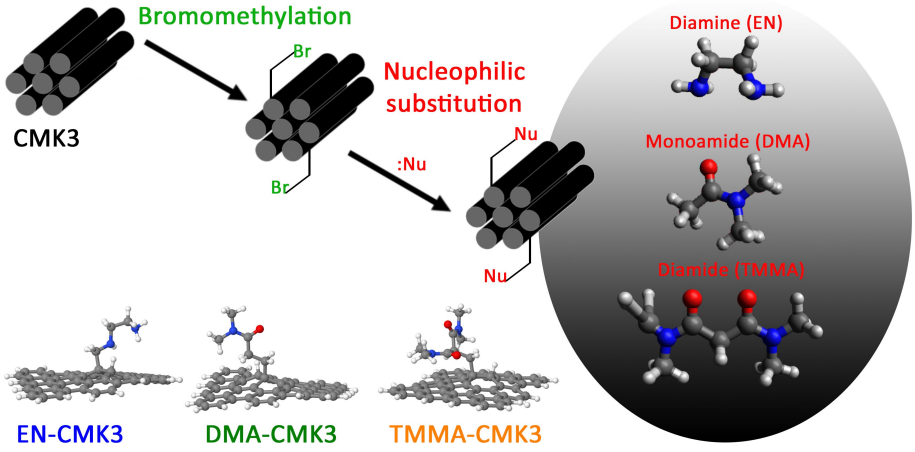

Figure 1. Depiction of the two-step surface functionalization process of CMK3: bromomethylation and subsequent nucleophilic substitution with diamine (EN-CMK3), monoamide (DMA-CMK3), or diamide (TMMA-CMK3) nucleophiles.

yields together with the non-negligible residual Br content (21–31 % of the original) suggest that these nucleophiles react with other surface functionality besides the bromomethyl groups to a fairly significant extent (*e.g.* condensation with an aldehyde or ketone for EN; addition to a carbonyl group for DMA).

To further elucidate the elemental compositions of the CMK3 surfaces, the functionalized carbons were investigated by XPS (Table S3). Consistent with the XRF and EA data, Br-CMK3 shows a large Br content that is significantly reduced, but not completely removed, upon EN, DMA, and TMMA substitution with a corresponding increase in the nitrogen signal. The relative residual Br contents of EN-, DMA-, and TMMA-CMK3 as determined by XPS match well with their residual Br loadings as determined by XRF (Table S1). EN-CMK3 exhibits a much higher nitrogen content than either amide-functionalized carbon, confirming its higher loading, while the amide samples have very similar levels, in line with their comparable nitrogen loadings (EA, Table S2). An increase in the oxygen content was also observed for DMA- and TMMA-CMK3, which is consistent with attaching carbonyl-containing amide groups to the surface. The lower oxygen content of EN-CMK3 relative to Br-CMK3 and CMK3 suggests a condensation reaction as the reason for the high yield of EN-CMK3 since such a reaction would eliminate oxygen (as water) from the carbon surface.

In the Br 3d XPS spectra (Figure 2a), Br-CMK3 exhibits a large bromine concentration with two distinct peaks at *ca.* 71 eV and 68 eV, which are associated with alkylbromides[31] and anionic bromides,[33] respectively. For the peak at 71 eV, its intensity decreases in the order TMMA-CMK3 > DMA-CMK3 > EN-CMK3, which reflects the trends in the XRF and EA measurements in terms of substitution efficiency (Table S1 and Table S2). For the peak at 68 eV, its intensity is similar across all modified CMK3 samples relative to the baseline noise, suggesting the presence of bromide anions trapped in the carbon pores after bromomethylation. The reaction conditions used for any nucleophilic substitution in this study apparently cannot dislodge these anions from the carbon. In the case of EN-CMK3, since its peak at 71 eV has negligible intensity, the residual Br content of this carbon as determined by XRF is likely anionic bromide.

In the N 1s spectra (Figure 2b), the higher intensity for EN-CMK3 relative to both amide-substituted samples is consistent with its higher yield and nitrogen content (Table S2). Most importantly, however, the peaks for the amide-functionalized CMK3 samples are also shifted to higher binding energies by *ca.* 1 eV, which is due to the electron withdrawing nature of the adjacent carbonyl group to the nitrogen atom; such a shift is consistent with an amide group relative to an amine.[34] This shift gives strong evidence for DMA and TMMA substitution of bromide as opposed to other nitrogen sources present in the substitution reaction such as the strong base used to form the amide nucleophile (LDA or LiHMDS, see experimental section). The complete lack of iodine from the tetrabutylammonium iodide (TBAI) catalyst and silicon from the LiHMDS base as determined by both XRF and XPS also supports amide attachment to the surface.

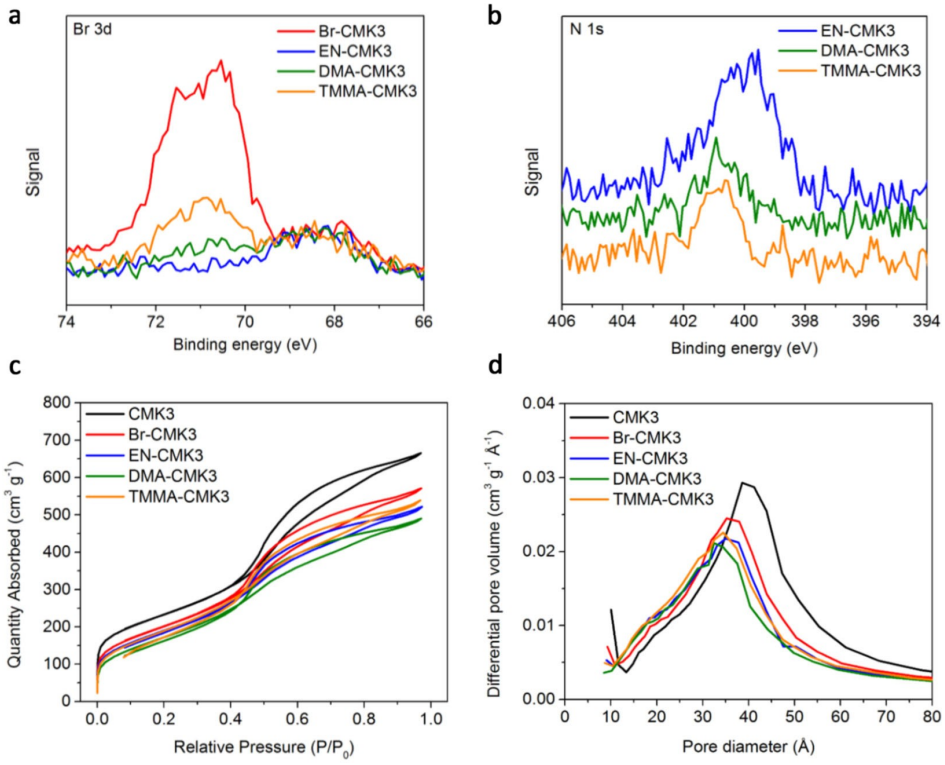

Figure 2. Characterization of the functionalized CMK3. X-ray photoelectron spectra (XPS) of the a) Br 3d and b) N 1s regions. In the N 1s spectra, the plots have been offset in signal intensity for clarity. c) Nitrogen adsorption-desorption isotherms and d) corresponding pore size distributions based on the adsorption isotherm.

The surface and electrochemical properties of the modified CMK3 samples were probed with nitrogen-sorption and cyclic voltammetry (CV). The underivatized CMK3 sample shows the greatest nitrogen adsorption capacity, which is decreased sequentially upon bromomethylation then substitution (Figure 2c). This shift is corroborated in that the highest BET surface areas, BJH pore volumes and diameter were found for CMK3, followed by Br-CMK3, then the EN- and amide-substituted samples (Table S4). This follows the trend of larger surface groups lead to lower nitrogen sorption capacity. In spite of the larger size of TMMA compared to either EN or DMA, TMMA-CMK3 was found to possess a relatively high surface area and pore volume, which is reflective of its lower surface group loading (Table S2). In the pore size distributions (Figure 2d), it is observed that the larger mesopores (>20 Å) of CMK3 are replaced with sequentially smaller pores in first Br-CMK3, then the substituted samples. The volume of the micropores (< 20 Å) also follows this trend. Overall, DMA-CMK3 experiences the largest decrease in porosity as evidenced by its lowest surface area and pore volume, however, the extent to which these values decrease relative to pristine CMK3 are minimal (*ca.* 20–25%) compared to other surface modification methods such as the oxidation and diazonium salt functionalization (*ca.* 50–90% decrease),[35,36] which underscores some of principal advantages of this two-step method: retention of porosity and negligible damage of the mesoporous carbon framework. Cyclic voltammograms with two Li–S electrolytes show very similar traces for all CMK3 samples (Figure S4). From this, we concluded that the reactions used to synthesize the functionalized carbons do not deleteriously affect the carbons' conductivity and that the surface-bound amine and amide groups are redox inactive under the voltages and conditions used. For the electrolyte containing lithium nitrate ($LiNO_3$), no significant change was observed in the nitrate reduction peak at low cell voltages, indicating that the surface groups do not impact nitrate reduction meaningfully.

The nature and strength of the interactions between the surface groups and various sulfur species were probed by density functional theory (DFT) calculations. The unmodified carbon surface was modelled with a $C_{54}H_{20}$ system consisting of 18 aromatic rings. To model the functionalized surfaces, two bonding motifs to $C_{54}H_{20}$ were used: face-bonding and edge-bonding. Details about the bonding motifs as well as the methods and models applied can be found in the experimental section. The interaction strength is modelled using the binding energy (BE) between either elemental sulfur (S_8) or a reduced sulfur species (Li_2S_n, $1 \leq n \leq 8$) and the surface of a CMK3 carbon, with or without surface groups. The optimized structures for the face-bonded and edge-bonded surface groups are shown in Figure S5 and Figure S6, respectively, and the corresponding BEs are shown in Table S5 and Table S6, respectively. The BEs for all sulfur species, surfaces, and bonding motifs are summarized in Figure 3.

One might expect *a priori* that S_8 would show the highest BE to the unmodified CMK3 surface given that both species are non-polar and hydrophobic, and in most cases this was found to be the case, but the slightly higher BE calculated for S_8 with DMA-CMK3 in the face-bonding motif shows that other effects (*e.g.* polarizability) could have a significant impact on the calculated BE. The complexity of potential interactions between the carbon surface and a given sulfur species is exemplified in that, upon reduction to either Li_2S_8 (face-bonding) or Li_2S_6 (edge-bonding), the dianionic LiPs actually shows a higher BE to the unmodified surface compared to neutral S_8. All other

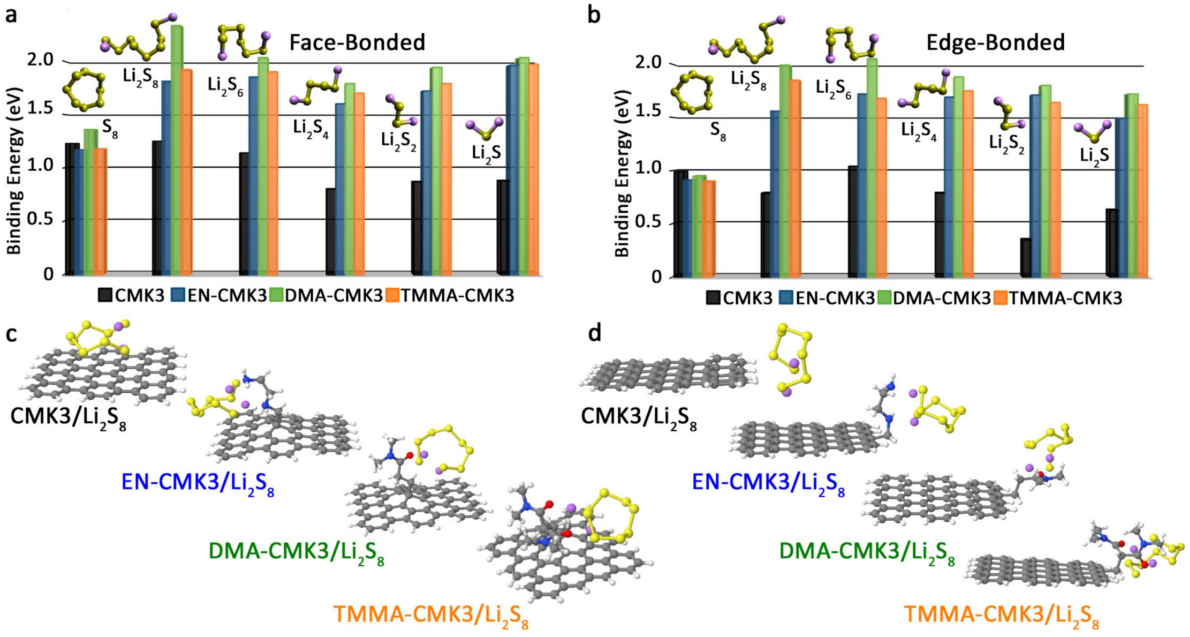

Figure 3. Binding energies between different sulfur species and an unfunctionalized (CMK3) or functionalized (EN-CMK3, DMA-CMK3, TMMA-CMK3) surface. Functional groups are either a) face-bonded or b) edge-bonded. Optimized structures between the surface and Li_2S_8 are shown for c) face-bonded and d) edge-bonded groups.

reduced sulfur-CMK3 combinations result in lower BEs relative to S_8-CMK3, indicating weaker interactions between the sulfur species and the unfunctionalized carbon surface as would be expected from a hydrophilic-hydrophobic perspective.

Undoubtedly, the biggest difference results from the interaction of reduced sulfur species and the modified CMK3 surfaces. By adding any of the three functional groups, the BE increases substantially, sometimes by a factor of 2 or more, over the CMK3 control. Thus, as expected, adding polar groups to the carbon surface can significantly enhance the interactions with polar sulfur species.[19] The higher BEs calculated for the functionalized carbons suggest that they will have a potential advantage at retaining the soluble LiPs near the cathode surface, which should facilitate their electrochemical conversion and limit their undesired diffusion to the Li anode during cell cycling. Importantly, the average increase in BE is similar between bonding motifs (1.8–2.6x over the control), suggesting that the nature of the bond to the surface has minimal impact on the reduced sulfur-surface group interactions. Among the functionalized surfaces, a trend is observed in the BEs in both bonding motifs for almost all reduced sulfur species: DMA-CMK3 > TMMA-CMK3 > EN-CMK3. These results are consistent with the previous report that found the highest BEs for carbonyl groups, since TMMA and DMA contain carbonyl groups whereas EN does not. The higher average BEs found with DMA-CMK3 over TMMA-CMK3 suggests that monoamides may bind reduced sulfur species better than diamides, despite the latter have twice as many carbonyls. One plausible explanation for this difference is the bulkiness and inflexibility of surface-bound TMMA, which could limit its potential binding modes to reduced sulfur species, thereby attenuating its BE relative to the smaller, more flexible DMA groups. Lastly, the average BE for each face-bonded surface is about 0.1–0.2 eV higher than the corresponding average BE for the edge-bonded groups, which could indicate that sulfur adsorption on the graphene face is inherently more favorable than edge adsorption.

To confirm the advantage of modifying the CMK3 surface, all carbons were used as cathodes for the adsorption of LiPs followed by testing in Li–S cells. Several methods exist to incorporate sulfur into the carbon host, including melt diffusion of sulfur at its low viscosity point (155 °C) and the catholyte system used in the previous study.[14,32,37,38] Melt diffusion of sulfur was found previously to significantly degrade the surface groups of EN-CMK3 so this method was not attempted. An alternative approach that avoids the high temperatures of melt diffusion is depositing a LiPs solution directly on the surface of the carbon electrode followed by gentle heating to evaporate the solvent.[39] Additionally, unlike a catholyte which contains LiPs in initial contact with both electrodes, the deposition with mild heating allows for any LiPs-surface group interactions to pre-form at the cathode before electrolyte addition and cell cycling, thereby potentially enhancing the LiPs adsorption to the carbon surface. Thus, we synthesized a 1 M Li_2S_8 solution in dimethoxyethane (DME) and drop casted it on the surface of pre-cut CMK3 cathodes with complete evaporation of the DME solvent, obtaining a final areal sulfur loading of *ca.* 3.3 mg cm^{-2} (see Experimental Section for further details). The electrolyte used was 1 M lithium bis(trifluoromethanesulfonyl)imide (LiTFSI) with 0.4 M lithium nitrate ($LiNO_3$) in a 1 : 1 by volume mixture of dimethoxyethane (DME) and dioxolane (DOL).

A schematic of the Li–S cell configuration using CMK3 electrodes with different functional groups is reported in Figure 4a. The Li_2S_8-impregnated CMK3 electrodes were incorporated into Li–S cells and were cycled at a rate of C/10 (C = 1675 mA g^{-1}, Figure 4b–e). During the first discharge (Figure 4b), the unmodified CMK3 carbon delivers a specific capacity of 1050 mAh g^{-1}, while the functionalized CMK3 carbons show similar capacities of *ca.* 1180 mAh g^{-1}. Improvements from the surface functionalization become much more apparent during the second cycle (Figure 4c). The DMA-CMK3 cell increases its specific capacity to 1460 mAh g^{-1}, while the EN-CMK3 and TMMA-CMK3 cells increase theirs to 1430 mAh g^{-1} and 1350 mAh g^{-1}, respectively. The CMK3 cell, meanwhile, shows a slightly lower capacity compared to its first cycle at 1000 mAh g^{-1}. The increase in capacity for the modified carbons is ascribed to more S_8 formation during charging, which permits additional sulfur reduction in latter cycles. The waveforms shown in Figure 4c and d support this claim in that the first discharge plateau at 2.4 V, which represents S_8 reduction to Li_2S_8, becomes pronounced during the second cycle. While the change in the first plateau occurs for all four cathodes, in the case of unfunctionalized CMK3, the second discharge plateau at 2.1 V becomes proportionally shorter, thereby decreasing its overall capacity slightly in the second cycle. Since the second plateau corresponds to Li_2S_n ($3 \leq n \leq 8$) conversion to Li_2S_2 and Li_2S,[11,16] its decreased length for CMK3 indicates a reduced interaction between its surface and LiPs relative to the modified CMK3 surfaces, while the functionalized carbons have the ability to convert a larger portion of Li_2S_n. This observation is consistent with the much lower BE calculated for CMK3 relative to its functionalized derivatives (Figure 3 and Table S5).

Upon prolonged cycling, the unfunctionalized CMK3 carbon shows the lowest specific capacity, stabilizing at 800 mAh g^{-1} around cycle 15, while the functionalized cathodes exhibit higher stabilized capacities for the first 100 cycles at *ca.* 1100 mAh g^{-1} (Figure 4d), in agreement with their enhanced BEs of the latter with Li_2S_n species (Figure 3). The similar performance among the three functionalized carbons suggests that the surface groups' relative BEs and their loadings may offset each other: higher BEs were found for the amide-modified surfaces, DMA-CMK3 and TMMA-CMK3, relative to EN-CMK3, but both of these have noticeably lower surface group loadings (Table S2). In other words, if the surface group loadings of DMA-CMK3 or TMMA-CMK3 could be increased to the level of EN-CMK3 (> 0.9 mmol g^{-1}) or greater, such carbons would potentially show an increase in Li–S battery performance. After the first 100 cycles, TMMA-CMK3 and EN-CMK3 show noticeable decreases in discharge capacity while DMA-CMK3 maintains a stable capacity through 150 cycles. This is consistent with its higher average BE compared to the other two surfaces. Interestingly, the unmodified CMK3 cathode

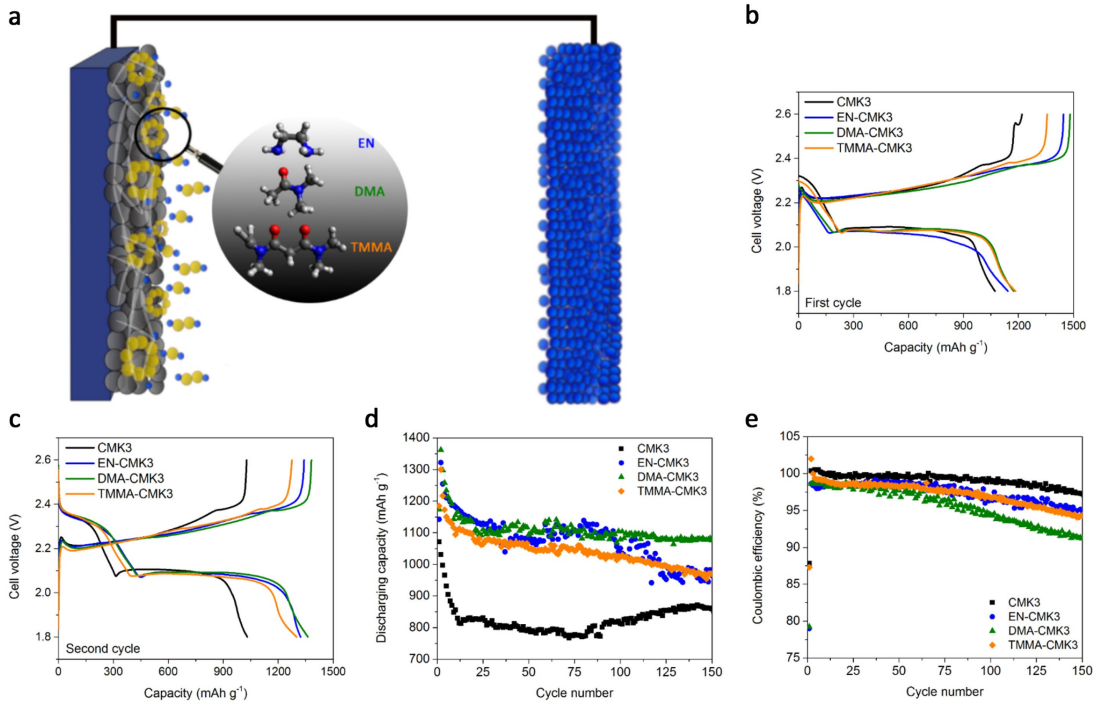

Figure 4. Battery configuration and galvanostatic cycling performance of Li–/S cells using CMK3 cathodes cycled between 1.8 – 2.6 V at a rate of C/10 (167.5 mA g^{-1}). a) Li–/S battery configuration including the use of functionalized CMK3. b) Voltage profiles for the 1st cycle and c) 2nd cycle. d) Specific discharging capacities versus cycle number and e) the corresponding Coulombic efficiencies.

shows a slight increase in capacity after the first 100 cycles, but its capacity is still lower than the modified cathodes.

In the Coulombic efficiencies (CEs, Figure 4e), since all cells started from Li_2S_8, a longer initial charge compared to discharge was needed to produce S_8 for the second cycle (Figure 4b), which results in initial Coulombic efficiencies (ICEs)[14,37] of *ca.* 87% for CMK3 and TMMA-CMK3 and *ca.* 78% for EN-CMK3 and DMA-CMK3. After the first cycle, the CEs increase to >97% for all Li–S cells with the CMK3 cell slightly outperforming its three functionalized derivatives. A plausible explanation for the higher CEs for CMK3 could be its lower capacity, meaning that less sulfur is reduced and oxidized in each cycle making it easier to achieve higher CEs. At around the 50th cycle, the functionalized cathodes show their CEs decreasing at a faster rate relative to the CMK3 control. There are a few possible reasons for this faster decrease: one, the amide and amine functional groups could slowly degrade during cycling, causing them to be less effective at binding to the LiPs; two, various electrolyte species could be deposited on the cathode surface during cycling (*e.g.* reduction of nitrate; Figure S4, right) and form a cathode electrolyte interface, which would also render the surface groups less effective; three, residual bromine species from bromomethylation (Figure 2a and Table S1) could slowly dissolve into the electrolyte, potentially causing corrosion and/or interfering with the sulfur electrochemistry; four, the higher capacities of the functionalized cathodes require a larger consumption of $LiNO_3$ additive at the Li side, which lowers the CEs during extending Li–/S cell cycling.[40]

3. Conclusions

Grafting polar organic functional groups to mesoporous carbon host is an efficient pathway to improve sulfur utilization in Li–/S batteries. Through density functional theory (DFT) calculations, we demonstrate that the presence of amine and amide at the host surface increases greatly the BEs between the carbon surface and the entire range of reduced sulfur species (Li_2S_n, $1 \leq n \leq 8$). Such an increase in the binding energies is postulated to promote the adsorption of Li_2S_n species, which, in turn, facilitates their electrochemical conversion at the surface of the carbon cathode during battery cycling. When the functionalized carbons are used as the host for sulfur in Li–S batteries, their higher BEs are realized in a *ca.* 30% increase in specific capacity and gravimetric energy density compared to unfunctionalized mesoporous host. We expect that the surface functionalization of mesoporous carbon host with a variety of polar groups opens up a new routes for re-designing Li–S host resulting in increased sulfur utilization and improved battery performance.

Experimental Section

Chemicals and carbon materials

All chemicals were purchased from Sigma-Aldrich and used as received except for lithium bis(trifluoromethanesulfonyl)imide (LiTFSI, <20 ppm H_2O, Solvionic) and polyvinylidene difluoride (PVdF, Arkema). Ordered mesoporous carbon CMK3 was purchased from ACS Materials and XC-72R (Vulcan) from The Fuel Cell Store.

Br-CMK3 and EN-CMK3 were synthesized with the modification of running bromomethylation to form Br-CMK3 on a 10-gram scale with all reagents scaled proportionally, as reported in our previous publication.[31] The synthesis of EN-CMK3 was ran on a 2-g scale with all reagents scaled proportionally. Br-CMK3 was dried at 60 °C for 2 hrs under vacuum for a minimum of 2 hrs before reaction with EN and amide nucleophiles. The tetrabutylammonium iodide (TBAI) catalyst was dried at 60 °C under vacuum before use. N,N,N′,N′-tetramethylmalonamide (TMMA) was dried with 3 Å molecular sieves overnight (24 hrs) and degassed with N_2 before use. CMK3 cathodes on aluminum current collectors were fabricated using the previously published procedure,[31] which is summarized here: a CMK3 sample was ball milled into a slurry with Vulcan and PVDF in a 8:1:1 weight ratio in an *N*-methyl-2-pyrrolidone (NMP) solvent and was poured onto an aluminum current collector. The slurry was coated with a doctor blade at 250 μm thickness followed by drying at room temperature (16 hrs) then 80 °C (2 hrs). The cathodes were cut into 10 mm diameter circles followed by a final drying step at 80 °C under vacuum (16 hrs) before immediate transfer into an argon-filled glovebox. The two battery electrolytes used in this study contain 1 M LiTFSI with or without 0.4 M lithium nitrate ($LiNO_3$) in a 1:1 by volume mixture in dimethoxyethane (DME) and dioxolane (DOL) and were made using the previously published procedure.[39]

Surface functionalization of CMK3 with amide nucleophiles

Unlike EN, the nucleophilic form of an amide must be generated under anhydrous, anaerobic conditions in the presence of Br-CMK3. This activation occurs *in situ* by taking advantage of the relatively acidic α C–H protons (CH_3 group adjacent to the carbonyl) of a tertiary amide like N,N-dimethylacetamide (DMA, pKa ~30), which can be deprotonated with a strong base such as lithium diisopropylamide (LDA, pKa of conjugate acid ~36) at low temperatures (−8 °C) in tetrahydrofuran (THF) solution to form an *enolate.* Amide enolates are stable when formed and are slow to undergo self-condensation, yet are reactive nucleophiles in substitution reactions. Meanwhile, the use of a bulky, non-nucleophilic base like LDA decreases its chances of direct bromide displacement on Br-CMK3. A >7-fold excess of LDA (relative to Br in Br-CMK3) is used to neutralize any acidic groups on the carbon surface (*e.g.* alcohols, carboxylic acids). A slight excess of DMA (*ca.* 2.5x relative to Br in Br-CMK3) is used to maximize the surface group yield. After enolate formation, the reaction is warmed to room temperature to increase the rate of substitution. A diamide functionality can be installed on the surface using a similar reaction with an *N*,*N*,*N*′,*N*′-tetramethylmalonamide (TMMA) enolate as the nucleophile. The additional amide carbonyl increases the acidity of the α C–H protons (CH_2 group) in TMMA (estimated pKa ~18-20) relative to DMA, meaning that a weaker, but less nucleophilic, base like lithium hexamethyldisilamide (LiHMDS, pKa of conjugate acid ~26) can be used. However, the additional amide group on TMMA also makes it bulkier and hence less reactive for substitutions. For this reason, a large excess (>13 equivalents relative to Br in Br-CMK3) of both LiHMDS and TMMA is used followed by heating to reflux (80 °C) to increase the rate and yield of this substitution reaction. For both amide enolates, a tetrabutylammonium iodide (TBAI) catalyst is used to further facilitate substitution. Further details related to these synthetic procedures are reported below and the synthetic processes are illustrated in Figures S1–S3.

Synthesis of DMA-CMK3

In an oven-dried, 250 mL round bottom flask were placed tetrabutylammonium iodide (TBAI, 150 mg, 0.4 mmol) and Br-CMK3 (2 g, 1.3 mmol Br). A magnetic stir bar was added, and the two side necks were sealed with rubber septa. The flask was placed in the fume hood and a hose adapter, attached to a N_2/vacuum manifold, was attached in the center neck. The flask was evacuated, flame dried, and refilled with N_2 three times. Under N_2, anhydrous tetrahydrofuran (THF, 50 mL) then anhydrous N,N-dimethylacetamide (DMA, 300 μL, 281 mg, 3.23 mmol) were added via syringe and the flask was cooled to *ca.* −8 °C in an acetone-ice bath. After stirring for 15 min, lithium diisopropylamide (LDA, 1 M in THF, 10 mL, 10 mmol) was added slowly over 5 min. The mixture was stirred for 30 min at −8 °C before removing the acetone-ice bath and stirring overnight (24 hrs) at room temperature. One of the rubber septa was removed and the reaction was quenched with ethanol (1 mL). The reaction was stirred for 5 min before water (1 mL) was added. The reaction was vacuum filtered, and the carbon was washed with water, 1:1 water-ethanol (v/v), ethanol, then acetone (2×100 mL each). The carbon product was dried in an air oven at 60 °C for 2 h before drying in vacuum at 60 °C overnight (16 hrs).

Synthesis of TMMA-CMK3

In an oven-dried, 250 mL round bottom flask were placed tetrabutylammonium iodide (TBAI, 150 mg, 0.4 mmol) and Br-CMK3 (2 g, 1.3 mmol Br). A magnetic stir bar was added and the two side necks were sealed with rubber septa. The flask was placed in the fume hood and a reflux condenser, attached to a N_2/vacuum manifold, was attached in the center neck. The flask was evacuated, flame dried, and refilled with N_2 three times. Under N_2, anhydrous THF (60 mL) then N,N,N′,N′-tetramethylmalonamide (TMMA, 3.1 mL, 3.41 g, 21.6 mmol) were added via syringe and the flask was cooled to *ca.* −8 °C in an acetone-ice bath. After stirring for 15 min, lithium hexamethyldisilamide (LiHMDS, 1 M in THF, 18 mL, 18 mmol) was added slowly over 15 min. Upon complete addition of LiHMDS, the reaction mixture became noticeably more viscous so additional THF was added (40 mL) followed by stirring for 15 min at −8 °C. The acetone-ice bath was removed and the mixture was stirred for 1 h at room temperature before heating to 80 °C overnight (24 hrs) in an oil bath. The reaction was allowed to cool to room temperature then one of the rubber septa was removed and the reaction was quenched with ethanol (2 mL). The reaction was stirred for 5 min before water (2 mL) was added. The reaction was vacuum filtered and was washed with water, 1:1 water-ethanol (v/v), ethanol, then acetone (2×100 mL each). The carbon product was dried in an air oven at 60 °C for 2 h before drying in vacuum at 60 °C overnight (16 hrs).

Modified carbon characterization

Determination of bromine loadings was performed on a Spectro Xepos HE XRF spectrometer using calibration data supplied by the manufacturer. Determination of nitrogen loadings for amine- and amide-functionalized carbons was performed by elemental analysis (EA) on an Elementar Vario MICRO Cube HCNS analyzer. X-ray photoelectron spectroscopy (XPS) was carried out on a Quantum 2000 scanning ESCA microprobe from Physical Electronics using Al K_α radiation (1486 eV) at an incidence angle of 45° relative to the sample surface. The Multipak Spectrum (ESCA) was used for analysis of the spectra and the binding energies for all spectra were referenced to the C 1s peak at 285 eV. Surface areas, pore volumes, and pore size distributions were measured by nitrogen-sorption using a TriStar 3000 instrument from Micromeritics. Unfunctionalized CMK3 was degassed for a minimum of 3 hrs at 200 °C under a N_2 flow. Functionalized CMK3 samples were degassed for a minimum of 16 hrs at 110 °C under a N_2 flow. The

surface areas were calculated using the Brunauer-Emmett-Teller (BET) algorithm and the pore volumes, diameters, and distributions were calculated using the Barrett-Joyner-Halenda (BJH) algorithm on the adsorption isotherm.

Density functional theory (DFT) calculations

The pristine carbon surface was simulated using a $C_{54}H_{20}$ model, consisting of 18 aromatic rings. To introduce a functional group to this model, two different bonding motifs were used. Before describing these motifs, it must be emphasized that, as an amorphous carbon, CMK3 has mixed sp^2/sp^3 hybridization and, as such, knowing exactly how the surface groups are bonded the amorphous carbon surface becomes difficult to state. The presence of a native oxide layer on CMK3 further complicates potential bonding arrangements to the surface. To simplify the surface binding, in the previous study on bromomethylation, the carbon surface was described as a graphitic sheet and the bromomethyl groups were proposed to be bonded to the edge oft he sheet as benzyl bromide.[31] The new C-C bond comes as result of formaldehyde substitution of a proton, which forms a benzyl alcohol intermediate. Subsequently, under the highly acidic conditions with HBr, the benzyl alcohol is transformed into a benzyl bromide. To model this bonding arrangement, one of the protons on the $C_{54}H_{20}$ model was substituted for a methylene (CH_2) group, which is in turn connected to the rest of the functional group. This bonding motif is referred to as *edge-bonding*.

The other bonding motif is also based on a graphitic sheet. This is performed by attaching the CH_2 group to the central carbon atom, which changes its hybridization from sp^2 to sp^3. However, unlike in edge-bonding, there is no proton on the central carbon atom that can be detached to balance the charge of the system. In this case, a hydrogen, effectively a hydride (H^-), was added to the neighboring carbon atom to maintain a neutral charge. This bonding motif is referred to as *face-bonding*.

The BEs between the eight resulting surfaces (four edge-bonded, four face-bonded) and the following sulfur species were calculated: S_8, Li_2S, Li_2S_2, Li_2S_4, Li_2S_6, and Li_2S_8. The charge and spin multiplicity for each system were 0 and 1, respectively. For each surface and sulfur species combination, a minimum of 5 different starting geometries were tested prior to geometry optimization, in order to determine the most favorable geometries. To reduce the computation time, all structures were preoptimized using a smaller basis set, 6-31G(d), prior to the final geometry optimization using 6-311++G(d,p). The M06-2X functional with Grimme dispersion corrections (D3), as implemented in Gaussian16 B.01 was used,[41] which has been shown to be appropriate for studies of graphene and carbon nanotubes.[42] The BEs were obtained by subtracting the total energy of the carbon layer-Li_2S_x system from the sum of the isolated carbon layer and Li_2S_x species, optimized separately: $BE = E_{carbon+LPS} - E_{carbon} - E_{LPS}$. To reduce the error related to the large difference in basis set size with and without the carbon layer, BSSE correction was considered by calculation of optimized geometries of separated species in the basis set of entire system, and the error was determined to be around 0.1 eV.

Polysulfide solution preparation and cathode impregnation

In an argon-filled glovebox, lithium metal (0.14 g, 20 mmol), sulfur (2.56 g, 80 mmol), dimethoxyethane (DME, 10 mL), and a small stir bar were placed in a dried 20 mL vial. The solution was heated at 80 °C with stirring for 4 hrs and a deep red solution was obtained. The final Li_2S_8 concentration was 1 M. In an argon-filled glove box, a pre-cut 10 mm diameter CMK3 cathode (0.785 cm^2) was placed on a hotplate at 80 °C. The 1 M Li_2S_8 solution in DME (10 μL, 10 μmol Li_2S_8) was added to the center of the cathode. The cathode was kept at 80 °C for a minimum of 5 min to completely evaporate the DME solvent. The areal sulfur loading was calculated to be ca. 3.3 mg cm^{-2} based on the amount of sulfur in the 10 μL of Li_2S_8 solution (2.56 mg) and the apparent surface area of the carbon cathode (0.785 cm^2).[39] The use of an impregnation method for adding the sulfur active materials at the electrode has main advantage of avoiding thermal synthesis which require the use of temperature higher than the boiling point of sulfur (155 °C), reducing the possibility of active material lost via evaporation and also minimizing possible damages of functional groups. Furthermore, this method gives the possibility of easily regulate the active material loading at the electrode.

Li–S battery fabrication and testing

CMK3 cathodes were tested in CR2032 type coin cells (Wellcos Co.) using 16 mm diameter polypropylene Celgard 2400 separator (Wellcos Co), 30 μL electrolyte (1 M LiTFSI with 0.4 M $LiNO_3$ in 1:1 DOL-DME), and 14 mm diameter lithium foil anodes. The CMK3 cathodes had been previously cut into 10 mm diameter circles and impregnated with the 1 M Li_2S_8 solution. The electrolyte-facing side of the lithium anode was scratched gently with plastic tweezers immediately before being used in a coin cell to remove any contaminants from the surface. The assembly order was cathode, 20 μL electrolyte, separator, 10 μL electrolyte, anode. Constant current battery cycling was conducted on a 580 Battery Tester System from Scribner Associates. Cells were cycled at a rate of 0.1 C (*i.e.* 0.428 mA) for 150 cycles. The voltage cut-offs were 2.6 and 1.8 V. All capacities and currents are normalized against the mass of sulfur. Coin cells for cyclic voltammetry (CV) were prepared as described here but without Li_2S_8 impregnation of the cathode and tested at 0.2 mV s^{-1} in a voltage range between 1.8 to 2.6 V. The current densities for CV are normalized against the apparent surface area of the CMK3 working electrode (0.785 cm^2).

Acknowledgements

The Swedish Energy Agency is gratefully acknowledged for project funding (project 37671–1, Next Generation Batteries). M.A and A. M acknowledge support from the Chalmers Areas of Advance Materials Science and Energy, FORMAS, and the Swedish Energy Agency. P.Joh. and P.Jan. also acknowledge Chalmers Battery Initiative, part of the profile Materials for Energy Applications jointly managed by the Areas of Advance Materials Science and Energy at Chalmers University of Technology. S.J.F and A.P. thank the following people: Prof. T. Daniel P. Stack at Stanford University (Stanford, CA, USA) for help with the bromomethylation reaction, Dr. Maksim Osipov (Stanford PhD 2014) for help with the amide substitution reactions, Dr. Juan Salvador Lezama Pacheco at Stanford for acquiring the XRF measurements, and Anne Wendel at Chalmers for acquiring the XPS spectra. Part of this work was conducted at Chalmers Materials Analysis Laboratory (CMAL) with muc help from Dr. Stefan Gustafsson. All calculations were carried out at the Wrocław Centre for Networking and Supercomputing, Grant number 346.

Conflict of Interest

The authors declare no conflict of interest.

Keywords: Li–S batteries · bromomethylation · high gravimetric energy density · density functional theory · polysulfides

[1] N. S. Choi, Z. Chen, S. A. Freunberger, X. Ji, Y. K. Sun, K. Amine, G. Yushin, L. F. Nazar, J. Cho, P. G. Bruce, *Angew. Chem. Int. Ed.* **2012**, *51*, 9994.
[2] N. Nitta, F. Wu, J. T. Lee, G. Yushin, *Mater. Today* **2015**, *18*, 252.
[3] J. M. Tarascon, M. Armand, *Nature* **2001**, *414*, 359.
[4] S. Chu, Y. Cui, N. Liu, *Nat. Mater.* **2017**, *16*, 16.
[5] A. Manthiram, Y. Fu, S.-H. Chung, C. Zu, Y.-S. Su, *Chem. Rev.* **2014**, *114*, 11751.
[6] Q. Pang, X. Liang, C. Y. Kwok, L. F. Nazar, *Nat. Energy* **2016**, *1*, 1.
[7] S. S. Zhang, *J. Power Sources* **2013**, *231*, 153.
[8] Y. X. Yin, S. Xin, Y. G. Guo, L. J. Wan, *Angew. Chem. Int. Ed.* **2013**, *52*, 13186.
[9] D. Bresser, S. Passerini, B. Scrosati, *Chem. Commun.* **2013**, *49*, 10545.
[10] P. P. R. M. L. Harks, C. B. Robledo, T. W. Verhallen, P. H. L. Notten, F. M. Mulder, *Adv. Energy Mater.* **2017**, *7*, 1.
[11] J. H. Kim, T. Kim, Y. C. Jeong, K. Lee, K. T. Park, S. J. Yang, C. R. Park, *Adv. Energy Mater.* **2015**, *5*, 1.
[12] S. E. Cheon, K. S. Ko, J. H. Cho, S. W. Kim, E. Y. Chin, H. T. Kim, *J. Electrochem. Soc.* **2003**, *150*, 796.
[13] X. Yang, X. Gao, Q. Sun, S. P. Jand, Y. Yu, Y. Zhao, X. Li, K. Adair, L. Y. Kuo, J. Rohrer, J. Liang, X. Lin, M. N. Banis, Y. Hu, H. Zhang, X. Li, R. Li, H. Zhang, P. Kaghazchi, T. K. Sham, X. Sun, *Adv. Mater.* **2019**, *31*, 1.
[14] D.-H. Lim, M. Agostini, F. Nitze, J. Manuel, J.-H. Ahn, A. Matic, *Sci. Rep.* **2017**, *7*, 6327.
[15] X. Ji, K. T. Lee, L. F. Nazar, *Nat. Mater.* **2009**, *8*, 500.
[16] L. F. Nazar, M. Cuisinier, Q. Pang, *MRS Bull.* **2014**, *39*, 436.
[17] J. Zhang, L. Zhou, H. Ming, Y. Wu, W. Wahyudi, Z. Cao, L. Cavallo, L. Wang, J. Ming, *Chem. Commun.* **2019**, *55*, 5713.
[18] M. Li, W. Wahyudi, P. Kumar, F. Wu, X. Yang, H. Li, L. J. Li, J. Ming, *ACS Appl. Mater. Interfaces* **2017**, *9*, 8047.
[19] M. Agostini, A. Matic, *Small* **2020**, *16*, 1905585.
[20] G. Zheng, Q. Zhang, J. J. Cha, Y. Yang, W. Li, Z. W. Seh, Y. Cui, *Nano Lett.* **2013**, *13*, 1265.
[21] Z. Li, L. Yin, *ACS Appl. Mater. Interfaces* **2015**, *7*, 4029.
[22] J. Pampel, T. P. Fellinger, *Adv. Energy Mater.* **2016**, *6*, 1.
[23] W. Shen, W. Fan, *J. Mater. Chem. A* **2013**, *1*, 999.
[24] J. Song, T. Xu, M. L. Gordin, P. Zhu, D. Lv, Y. B. Jiang, Y. Chen, Y. Duan, D. Wang, *Adv. Funct. Mater.* **2014**, *24*, 1243.
[25] F. Sun, J. Wang, H. Chen, W. Li, W. Qiao, D. Long, L. Ling, *ACS Appl. Mater. Interfaces* **2013**, *5*, 5630.
[26] A. Stein, Z. Wang, M. A. Fierke, *Adv. Mater.* **2009**, *21*, 265.
[27] C. Liang, Z. Li, S. Dai, *Angew. Chem. Int. Ed.* **2008**, *47*, 3696.
[28] R. L. McCreery, *Chem. Rev.* **2008**, *108*, 2646.
[29] M. R. Benzigar, S. N. Talapaneni, S. Joseph, K. Ramadass, G. Singh, J. Scaranto, U. Ravon, K. Al-Bahily, A. Vinu, *Chem. Soc. Rev.* **2018**, *47*, 2680.
[30] Z. W. Seh, Q. Zhang, W. Li, G. Zheng, H. Yao, Y. Cui, *Chem. Sci.* **2013**, *4*, 3673.
[31] S. J. Fretz, C. T. Lyons, E. Levin, A. E. C. Palmqvist, T. D. P. Stack, *J. Mater. Chem. A* **2019**, *7*, 20013.
[32] M. Agostini, D. H. Lim, M. Sadd, J.-Y. Hwang, S. Brutti, J. Heo, J.-H. Ahn, Y.-K. Sun, A. Matic, *ChemSusChem* **2018**, *11*, 2981.
[33] J. Li, L. Vaisman, G. Marom, J. K. Kim, *Carbon* **2007**, *45*, 744.
[34] D. Beamson, G. Briggs, *High resolution XPS of organic polymers: the Scienta ESCA300 database / G. Beamson and D. Briggs.*; Chichester [England]; New York: Wiley, c1992., 1992.
[35] A. Jaffe, A. Saldivar Valdes, H. I. Karunadasa, *Chem. Mater.* **2015**, *27*, 3568.
[36] X. Wang, R. Liu, M. M. Waje, Z. Chen, Y. Yan, K. N. Bozhilov, P. Feng, *Chem. Mater.* **2007**, *19*, 2395.
[37] M. Agostini, D. J. Lee, B. Scrosati, Y. K. Sun, J. Hassoun, *J. Power Sources* **2014**, *265*, 14.
[38] A. Manthiram, Y. Fu, Y. S. Su, *Acc. Chem. Res.* **2013**, *46*, 1125.
[39] M. Agostini, J. Hwang, H. M. Kim, P. Bruni, S. Brutti, F. Croce, A. Matic, Y.-K. Sun, *Adv. Energy Mater.* **2018**, *8*, 1801560.
[40] M. Agostini, M. Sadd, S. Xiong, C. Cavallo, J. Heo, J. H. Ahn, A. Matic, *ChemSusChem* **2019**, *12*, 4176.
[41] D. J. F. M. J. Frisch, G. W. Trucks, H. B. Schlegel, G. E. Scuseria, M. A. Robb, J. R. Cheeseman, G. Scalmani, V. Barone, G. A. Petersson, H. Nakatsuji, X. Li, M. Caricato, A. V. Marenich, J. Bloino, B. G. Janesko, R. Gomperts, B. Mennucci, H. P. Hratchian, J. V., Gaussian 16, Revision B.01 **2016**.
[42] A. Ramraj, I. H. Hillier, M. A. Vincent, N. A. Burton, *Chem. Phys. Lett.* **2010**, *484*, 295.

Manuscript received: February 5, 2020
Revised manuscript received: March 11, 2020
Accepted manuscript online: March 12, 2020
Version of record online: April 8, 2020